

# GHIL-Glue: Hierarchical Control with Filtered Subgoal Images

Anonymous Author(s)

Affiliation

Address

email

1           **Abstract:** Image and video generative models that are pre-trained on Internet-  
2 scale data can increase the generalization capacity of robot learning systems.  
3 These models can function as high-level planners, generating intermediate sub-  
4 goals for low-level goal-conditioned policies to reach. However, the performance  
5 of these systems can be bottlenecked by the interface between generative mod-  
6 els and low-level controllers. Generative models may predict photorealistic yet  
7 physically infeasible frames. Low-level policies may also be sensitive to subtle  
8 visual artifacts in generated goal images. This paper addresses these facets  
9 of generalization, providing an interface to “glue together” language-conditioned  
10 image or video prediction models with low-level goal-conditioned policies. Our  
11 method, Generative Hierarchical Imitation Learning-Glue (GHIL-Glue), filters  
12 out subgoals that do not lead to task progress and improves the robustness of goal-  
13 conditioned policies to generated subgoals with harmful visual artifacts. GHIL-  
14 Glue achieves a new state-of-the-art on the CALVIN simulation benchmark for  
15 policies using observations from a single RGB camera. GHIL-Glue also outper-  
16 forms other generalist robot policies across 3/4 language-conditioned manipula-  
17 tion tasks testing zero-shot generalization on a physical robot. Additional details  
18 are available at <https://generative-hierarchical-glue.github.io>.

19           **Keywords:** Hierarchical Imitation Learning, Image Generation, Video Prediction

## 20   1 Introduction

21 As Internet-scale foundation models achieve success in computer vision and natural language pro-  
22 cessing, a central question arises for robot learning: how can Internet-scale models enable embodied  
23 behavior generalization? While one approach is to collect increasingly large action-labeled robot  
24 manipulation training datasets [1, 2, 3], video datasets (without actions) from the Internet are vastly  
25 larger. However, while videos may be useful for inferring the steps in a task, such as how the objects  
26 should be moved, or which parts of an object to manipulate (e.g., grabbing a cup by the handle), they  
27 are less useful for learning details about low-level control. For example, it is difficult to infer the  
28 actions for controlling a robot’s fingers from videos of humans performing manipulation tasks. One  
29 promising solution to this challenge is to employ a hierarchical approach [4, 5]: infer high-level sub-  
30 goal images using models trained on Internet-scale videos, and then fill in the fine-grained motions  
31 with low-level policies trained on robot data (see appendix A for a discussion of related work).

32 While this general approach has seen success in prior robotic manipulation work [6, 4, 7, 5, 8, 9],  
33 the interface between the high-level planner generating subgoals and the low-level policy that must  
34 reach these subgoals can be brittle. First, generative models may occasionally sample subgoals that  
35 do not progress towards completing a given language instruction. If one such “off-task” subgoal is  
36 followed, it can have a compounding errors effect, leading to subsequent subgoals being increasingly  
37 “off-task.” Second, even if the generated subgoals lead to task progress, they can contain subtle  
38 visual artifacts that degrade the performance of a naively trained low-level policy.



**Figure 1: GHIL-Glue.** We consider language-conditioned image and video prediction models that can generate multiple subgoals. GHIL-Glue has two components: augmentation de-synchronization (top) and subgoal filtering (bottom). **Subgoal filtering:** We train a classifier to identify which subgoal is most likely to progress towards completing the language instruction. This subgoal and the image observation are then passed to the low-level policy to choose a robot action. **Augmentation de-synchronization:** The distribution shift between subgoals sampled from the robot dataset during training and those sampled from the generative model during inference can degrade low-level policy and subgoal classifier performance. To robustify the low-level policy and subgoal classifier to artifacts in generated subgoals, we explicitly de-synchronize the image-augmentations applied to the current state (State Aug) and the sampled goal (Subgoal Aug).

39 To address these issues, we propose Generative Hierarchical Imitation Learning-Glue (GHIL-Glue)  
40 (fig. 1), a method to *robustly* “glue” together image or video generative models to a low-level robotic  
41 control policy. **First**, we filter out “off-task” subgoals that are physically inconsistent with the com-  
42 manded language instruction. We do this by training a subgoal classifier to predict the likelihood  
43 of the transition between the current state and a given subgoal resulting in progress towards com-  
44 pleting the provided language instruction. We then sample a number of candidate subgoals from the  
45 generative model and choose the subgoal with the highest classifier ranking. **Second**, we identify  
46 a simple yet non-obvious data augmentation practice to robustify the low-level policy and subgoal  
47 classifier to visual artifacts in the generated subgoals. While image augmentations are ubiquitous in  
48 robot learning methods, our key finding is that the standard way of applying image augmentations  
49 does not make low-level policies robust to visual artifacts in generated subgoal images. Experiments  
50 on the CALVIN [10] simulation benchmark and four language-conditioned tasks on the Bridge V2  
51 physical robot platform [11] suggest that GHIL-Glue improves upon prior SOTA methods for zero-  
52 shot generalization while adding minimal additional algorithmic complexity.

## 53 2 GHIL-Glue

### 54 2.1 Subgoal Filtering

55 The image and video generative models we consider are first pre-trained on general Internet-scale  
56 image and video data, and then fine-tuned on a modest amount of robot data (see appendix B for  
57 a detailed description of the problem setting we consider). A common failure mode we observe  
58 across different models is that, while executing a task, the model begins to go “off-task,” generating  
59 subgoals that are consistent with the current image observation but that do not progress towards com-  
60 pleting the language instruction  $l$ . We hypothesize that this is due to the distribution shift between  
61 the Internet image and video pre-training data and the robot data they are fine-tuned on.

62 To address this challenge, we train a subgoal classifier  $f_\theta(s, g, l)$  on a language-conditioned dataset  
63 of trajectories  $\mathcal{D}_l$  that predicts the probability that the transition between the current image ob-  
64 servation  $s$  and the next subgoal  $g$  makes progress towards completing language instruction  $l$ .  
65 During training, we sample positive examples of state-goal transitions for  $l$  from the set of tra-  
66 jectories that successfully complete the instruction. We construct negative examples in the fol-  
67 lowing three ways: **1) Wrong Instruction:**  $(s, g, l')$  where  $l'$  is sampled from a different transi-  
68 tion than  $s$  and  $g$ , **2) Wrong Goal Image:**  $(s, g', l)$  where  $g'$  is sampled from a different transi-  
69 tion than  $s$  and  $l$ , and **3) Reverse Direction:**  $(g, s, l)$ , where the order of the current image  
70 observation and the subgoal image have been switched. We refer to this dataset of negative ex-  
71 amples constructed from  $\mathcal{D}_l$  as  $\mathcal{D}_l^-$ . We then train the subgoal classifier by minimizing the bi-  
72 nary cross entropy loss between the positive examples and the constructed negative examples:

73  $\mathcal{J}(\theta) = \mathbb{E}_{(s,g,l) \sim \mathcal{D}_l} [\log(f_\theta(s, g, l))] + \mathbb{E}_{(s^-, g^-, l^-) \sim \mathcal{D}_l^-} [\log(1 - f_\theta(s^-, g^-, l^-))]$ . At inference,  
74 given a set of  $K$  subgoals predicted by the image or video model, GHIL-Glue selects the subgoal  
75 with the highest classifier ranking to the low-level policy for conditioning.

## 76 2.2 Image Augmentation De-Synchronization

77 For both the low-level goal-conditioned policy and the subgoal classifier, each training sample in-  
78 cludes two images: the current state  $s$  and the corresponding goal  $g$ . Applying image augmentation  
79 procedures during training is a standard approach in image-based robot learning methods [12] to  
80 improve the robustness of learned models to distribution shifts between their training and evaluation  
81 domains. Standard practice is to sample augmentation parameters  $\hat{\phi}$  and apply them to all images  
82 in a given training sample [4, 13], which corresponds to applying the same  $\hat{\phi}$  to both  $s$  and  $g$ . In  
83 a non-hierarchical policy setting, this makes sense, because at inference time  $s$  and  $g$  will both be  
84 sampled from the camera observations of the current environment instantiation. However, when  
85 using an image or video prediction model for subgoal generation, at inference time the observations  
86 will come from the environment, but the goals will be generated by the image or video prediction  
87 model. There will often be differences in the visual artifacts between a camera observation  $s$  and the  
88 corresponding generated subgoal image  $g$ , such as differences in color, contrast, blurriness, and the  
89 shapes of objects, which can degrade the performance of low-level policies and subgoal classifiers.  
90 To encourage robustness to this distribution shift, we sample separate augmentation parameters for  
91  $s$  and  $g$ , denoted by  $\hat{\phi}_s$  and  $\hat{\phi}_g$  (i.e., we de-synchronize the image augmentations applied to  $s$  and  
92  $g$ ). Concretely, for each  $s$  and  $g$  pair sampled during training, a different random crop, brightness,  
93 contrast, saturation, and hue shift are applied to  $s$  than are applied to  $g$ . This forces the low-level  
94 policy and the subgoal classifier to be robust to differences in visual artifacts between  $s$  and  $g$ . See  
95 appendix C for additional discussion of image augmentation de-synchronization.

## 96 3 Experiments

### 97 3.1 Experimental Domains

98 **Simulation Experiment Setup:** Simulation experiments are performed in the CALVIN [10] bench-  
99 mark, which focuses on long-horizon language-conditioned robot manipulation. We follow the same  
100 protocol as in [4], and train on data from three environments (A, B, and C) and test policies on a  
101 fully unseen environment (D). The held-out environment (D) contains unseen desk and object colors,  
102 positions, and shapes. See appendix D for a visualization of the CALVIN environment.

103 **Physical Experiment Setup:** Physical experiments are performed with the Bridge V2 [11] ex-  
104 periment setup with a WidowX250 robot. We use the same datasets as in [4] for training both the  
105 high-level image prediction model and the low-level goal-conditioned policy. The Bridge V2 dataset  
106 contains 45K language-annotated trajectories, which are used for the language-labeled robot dataset  
107  $\mathcal{D}_{l,a}$ . The remaining 15K trajectories are used for the action-only dataset  $\mathcal{D}_a$ . As in [4], we use a  
108 filtered version of the Something-Something V2 dataset [14] with the same filtering scheme as in [4]  
109 (resulting in 75K video clips) as our video-only dataset  $\mathcal{D}_l$ . We test our policies on four tasks on four  
110 different cluttered table top scenes (fig. 2) on the Bridge V2 physical robot platform. These environ-  
111 ments require generalizing to novel scenes, with novel objects, and with novel language commands  
112 that are not seen in the Bridge V2 dataset. See appendix D for visualizations of the evaluation set-up.

### 113 3.2 Comparison Algorithms

114 We study the impact of applying GHIL-Glue to two SOTA hierarchical imitation learning algo-  
115 rithms: SuSIE [4] and UniPi [5]. We use either 4 or 8 candidate subgoals for subgoal filtering (see  
116 appendix J for details). We also compare GHIL-Glue to a flat language-conditioned diffusion policy  
117 (LCBC Diffusion Policy). Finally, we consider ablations where we separately study the impact of  
118 each of our proposed contributions: subgoal filtering (section 2.1) and de-synchronizing augmen-

tations (section 2.2). For physical experiments, we additionally compare to OpenVLA [15], which is trained on the Open X-Embodiment dataset [2] (which includes the Bridge V2 dataset). See appendix E for a detailed description of each of these algorithms.

### 3.3 Experimental Results

| Method                                     | Tasks completed in a row |              |              |              |              |             |
|--|--------------------------|--------------|--------------|--------------|--------------|-------------|
|  | 1                        | 2            | 3            | 4            | 5            | Avg. Len.   |
| LCBC Diffusion Policy                      | 68.5%                    | 43.0%        | 22.5%        | 11.0%        | 6.8%         | 1.52        |
| SuSIE [4]                                  | 89.8%                    | 75.0%        | 57.5%        | 41.8%        | 29.8%        | 2.94        |
| GHIL-Glue (SuSIE) - Aug De-sync Only       | 95.2%                    | 84.0%        | 69.5%        | 56.0%        | 46.2%        | 3.51        |
| GHIL-Glue (SuSIE) - Subgoal Filtering Only | 88.5%                    | 75.5%        | 56.2%        | 43.0%        | 32.5%        | 2.96        |
| GHIL-Glue (SuSIE)                          | <b>95.2%</b>             | <b>88.5%</b> | <b>73.2%</b> | <b>62.5%</b> | <b>49.8%</b> | <b>3.69</b> |
| UniPi [5]                                  | 56.8%                    | 28.3%        | 12.0%        | 3.5%         | 1.5%         | 1.02        |
| GHIL-Glue (UniPi) - Aug De-sync Only       | 60.2%                    | 29.5%        | 12.5%        | 5.5%         | 1.8%         | 1.1         |
| GHIL-Glue (UniPi) - Subgoal Filtering Only | 69.5%                    | 40.0%        | 15.8%        | 6.5%         | 4.2%         | 1.36        |
| GHIL-Glue (UniPi)                          | <b>75.2%</b>             | <b>44.8%</b> | <b>19.7%</b> | <b>11.2%</b> | <b>5.5%</b>  | <b>1.56</b> |

**Table 1: CALVIN: Simulation Results.** Success rates on the validation tasks from the held-out D environment of the CALVIN zero-shot generalization challenge averaged across 4 random seeds. Applying GHIL-Glue to SuSIE and UniPi significantly improves performance over their respective base methods. GHIL-Glue (SuSIE) significantly outperforms all other methods, achieving a new state-of-the-art on the CALVIN benchmark for policies using observations from a single RGB camera.

|         | Task                        | OpenVLA [15] | SuSIE [4] | GHIL-Glue (SuSIE) |
|---------|-----------------------------|--------------|-----------|-------------------|
| Scene A | Put Sushi On Towel          | 22/30        | 19/30     | <b>28/30</b>      |
| Scene B | Put Red Bell Pepper in Bowl | 14/30        | 12/30     | <b>16/30</b>      |
| Scene C | Open Drawer                 | <b>23/30</b> | 19/30     | 22/30             |
| Scene D | Put Sushi in Bowl           | 15/30        | 15/30     | <b>18/30</b>      |

**Table 2: Bridge V2 Physical Experiments Results.** Success rates across four tasks on four physical robot scenes (pictured in fig. 2) that test zero-shot generalization to novel objects, novel language commands, and novel scene configurations. GHIL-Glue applied to SuSIE outperforms SuSIE across all tasks and outperforms OpenVLA on 3 out of 4 tasks.

**Simulation Experiments:** We present results on the CALVIN benchmark in table 1. Applying GHIL-Glue yields significant improvements for SuSIE and UniPi, increasing the average successful task sequence length from **2.94** to **3.69** for SuSIE and from **1.02** to **1.56** for UniPi. **GHIL-Glue (SuSIE) achieves a new SOTA on CALVIN** for policies that use single RGB camera observations. See appendix F for additional discussion of results on CALVIN.

**Physical Experiments:** We present results (table 2) comparing GHIL-Glue (SuSIE) to OpenVLA and SuSIE across four environments on the Bridge V2 robot platform that require interacting with a number of objects on a cluttered table (fig. 2). GHIL-Glue applied to SuSIE outperforms SuSIE across all tasks and outperforms OpenVLA, a 7-billion parameter SOTA VLA, on 3 out of 4 tasks. Significantly, the baseline SuSIE implementation does not outperform OpenVLA on a single task, whereas **GHIL-Glue (SuSIE) outperforms OpenVLA on 3 out of 4 tasks**, demonstrating that hierarchical goal conditioned architectures with well-tuned interfaces between the high and low-level policies can outperform SOTA VLA methods on zero-shot generalization tasks. See appendix F for additional discussion of results and appendix I for qualitative analysis of success and failure cases.

## 4 Conclusion

We present GHIL-Glue, a method for better aligning image and video prediction models and low-level control policies for hierarchical imitation learning. Our key insight is that while image and video foundation models can generate highly realistic subgoals for goal-conditioned policy learning, when generalizing to novel environments, the generated images are prone to containing visual artifacts and can be inconsistent with the task the robot is commanded to perform. GHIL-Glue provides two simple ideas to address these challenges, significantly improving zero-shot generalization performance over prior work in the CALVIN simulation benchmark and in physical experiments.

145 **References**

- 146 [1] S. Dasari, F. Ebert, S. Tian, S. Nair, B. Bucher, K. Schmeckpeper, S. Singh, S. Levine, and  
147 C. Finn. Robonet: Large-scale multi-robot learning. In *Conference on Robot Learning (CoRL)*,  
148 2019.
- 149 [2] O. X.-E. Collaboration, A. O'Neill, A. Rehman, A. Maddukuri, A. Gupta, A. Padalkar, A. Lee,  
150 A. Pooley, A. Gupta, A. Mandlekar, A. Jain, A. Tung, A. Bewley, A. Herzog, A. Irpan,  
151 A. Khazatsky, A. Rai, A. Gupta, A. Wang, A. Kolobov, A. Singh, A. Garg, A. Kembhavi,  
152 A. Xie, A. Brohan, A. Raffin, A. Sharma, A. Yavary, A. Jain, A. Balakrishna, A. Wahid,  
153 B. Burgess-Limerick, B. Kim, B. Schölkopf, B. Wulfe, B. Ichter, C. Lu, C. Xu, C. Le, C. Finn,  
154 C. Wang, C. Xu, C. Chi, C. Huang, C. Chan, C. Agia, C. Pan, C. Fu, C. Devin, D. Xu,  
155 D. Morton, D. Driess, D. Chen, D. Pathak, D. Shah, D. Büchler, D. Jayaraman, D. Kalash-  
156 nikov, D. Sadigh, E. Johns, E. Foster, F. Liu, F. Ceola, F. Xia, F. Zhao, F. V. Frujeri, F. Stulp,  
157 G. Zhou, G. S. Sukhatme, G. Salhotra, G. Yan, G. Feng, G. Schiavi, G. Berseth, G. Kahn,  
158 G. Yang, G. Wang, H. Su, H.-S. Fang, H. Shi, H. Bao, H. B. Amor, H. I. Christensen, H. Fu-  
159 ruta, H. Walke, H. Fang, H. Ha, I. Mordatch, I. Radosavovic, I. Leal, J. Liang, J. Abou-Chakra,  
160 J. Kim, J. Drake, J. Peters, J. Schneider, J. Hsu, J. Bohg, J. Bingham, J. Wu, J. Gao, J. Hu,  
161 J. Wu, J. Wu, J. Sun, J. Luo, J. Gu, J. Tan, J. Oh, J. Wu, J. Lu, J. Yang, J. Malik, J. Silvério,  
162 J. Hejna, J. Booher, J. Tompson, J. Yang, J. Salvador, J. J. Lim, J. Han, K. Wang, K. Rao,  
163 K. Pertsch, K. Hausman, K. Go, K. Gopalakrishnan, K. Goldberg, K. Byrne, K. Oslund,  
164 K. Kawaharazuka, K. Black, K. Lin, K. Zhang, K. Ehsani, K. Lekkala, K. Ellis, K. Rana,  
165 K. Srinivasan, K. Fang, K. P. Singh, K.-H. Zeng, K. Hatch, K. Hsu, L. Itti, L. Y. Chen, L. Pinto,  
166 L. Fei-Fei, L. Tan, L. J. Fan, L. Ott, L. Lee, L. Weihs, M. Chen, M. Lepert, M. Memmel,  
167 M. Tomizuka, M. Itkina, M. G. Castro, M. Spero, M. Du, M. Ahn, M. C. Yip, M. Zhang,  
168 M. Ding, M. Heo, M. K. Srirama, M. Sharma, M. J. Kim, N. Kanazawa, N. Hansen, N. Heess,  
169 N. J. Joshi, N. Suenderhauf, N. Liu, N. D. Palo, N. M. M. Shafiuallah, O. Mees, O. Kroemer,  
170 O. Bastani, P. R. Sanketi, P. T. Miller, P. Yin, P. Wohlhart, P. Xu, P. D. Fagan, P. Mitrano,  
171 P. Sermanet, P. Abbeel, P. Sundaresan, Q. Chen, Q. Vuong, R. Rafailov, R. Tian, R. Doshi,  
172 R. Mart'in-Mart'in, R. Baijal, R. Scalise, R. Hendrix, R. Lin, R. Qian, R. Zhang, R. Men-  
173 donca, R. Shah, R. Hoque, R. Julian, S. Bustamante, S. Kirmani, S. Levine, S. Lin, S. Moore,  
174 S. Bahl, S. Dass, S. Sonawani, S. Song, S. Xu, S. Haldar, S. Karamcheti, S. Adebola, S. Guist,  
175 S. Nasiriany, S. Schaal, S. Welker, S. Tian, S. Ramamoorthy, S. Dasari, S. Belkhale, S. Park,  
176 S. Nair, S. Mirchandani, T. Osa, T. Gupta, T. Harada, T. Matsushima, T. Xiao, T. Kollar, T. Yu,  
177 T. Ding, T. Davchev, T. Z. Zhao, T. Armstrong, T. Darrell, T. Chung, V. Jain, V. Vanhoucke,  
178 W. Zhan, W. Zhou, W. Burgard, X. Chen, X. Chen, X. Wang, X. Zhu, X. Geng, X. Liu,  
179 X. Liangwei, X. Li, Y. Pang, Y. Lu, Y. J. Ma, Y. Kim, Y. Chebotar, Y. Zhou, Y. Zhu, Y. Wu,  
180 Y. Xu, Y. Wang, Y. Bisk, Y. Dou, Y. Cho, Y. Lee, Y. Cui, Y. Cao, Y.-H. Wu, Y. Tang, Y. Zhu,  
181 Y. Zhang, Y. Jiang, Y. Li, Y. Li, Y. Iwasawa, Y. Matsuo, Z. Ma, Z. Xu, Z. J. Cui, Z. Zhang,  
182 Z. Fu, and Z. Lin. Open X-Embodiment: Robotic learning datasets and RT-X models. 2024.
- 183 [3] A. Khazatsky, K. Pertsch, S. Nair, A. Balakrishna, S. Dasari, S. Karamcheti, S. Nasiriany,  
184 M. K. Srirama, L. Y. Chen, K. Ellis, P. D. Fagan, J. Hejna, M. Itkina, M. Lepert, Y. J. Ma,  
185 P. T. Miller, J. Wu, S. Belkhale, S. Dass, H. Ha, A. Jain, A. Lee, Y. Lee, M. Memmel, S. Park,  
186 I. Radosavovic, K. Wang, A. Zhan, K. Black, C. Chi, K. B. Hatch, S. Lin, J. Lu, J. Mer-  
187 cat, A. Rehman, P. R. Sanketi, A. Sharma, C. Simpson, Q. Vuong, H. R. Walke, B. Wulfe,  
188 T. Xiao, J. H. Yang, A. Yavary, T. Z. Zhao, C. Agia, R. Baijal, M. G. Castro, D. Chen, Q. Chen,  
189 T. Chung, J. Drake, E. P. Foster, J. Gao, D. A. Herrera, M. Heo, K. Hsu, J. Hu, D. Jackson,  
190 C. Le, Y. Li, K. Lin, R. Lin, Z. Ma, A. Maddukuri, S. Mirchandani, D. Morton, T. Nguyen,  
191 A. O'Neill, R. Scalise, D. Seale, V. Son, S. Tian, E. Tran, A. E. Wang, Y. Wu, A. Xie, J. Yang,  
192 P. Yin, Y. Zhang, O. Bastani, G. Berseth, J. Bohg, K. Goldberg, A. Gupta, A. Gupta, D. Ja-  
193 yaraman, J. J. Lim, J. Malik, R. Martín-Martín, S. Ramamoorthy, D. Sadigh, S. Song, J. Wu,  
194 M. C. Yip, Y. Zhu, T. Kollar, S. Levine, and C. Finn. Droid: A large-scale in-the-wild robot  
195 manipulation dataset. 2024.

- 196 [4] K. Black, M. Nakamoto, P. Atreya, H. Walke, C. Finn, A. Kumar, and S. Levine. Zero-  
197 shot robotic manipulation with pretrained image-editing diffusion models. *arXiv preprint*  
198 *arXiv:2310.10639*, 2023.
- 199 [5] Y. Du, S. Yang, B. Dai, H. Dai, O. Nachum, J. Tenenbaum, D. Schuurmans, and P. Abbeel.  
200 Learning universal policies via text-guided video generation. *Advances in Neural Information*  
201 *Processing Systems*, 36, 2024.
- 202 [6] I. Kapelyukh, V. Vosylius, and E. Johns. Dall-e-bot: Introducing web-scale diffusion models  
203 to robotics. *IEEE Robotics and Automation Letters*, 2023.
- 204 [7] Y. Du, M. Yang, P. Florence, F. Xia, A. Wahid, B. Ichter, P. Sermanet, T. Yu, P. Abbeel, J. B.  
205 Tenenbaum, et al. Video language planning. *arXiv preprint arXiv:2310.10625*, 2023.
- 206 [8] A. Ajay, S. Han, Y. Du, S. Li, A. Gupta, T. Jaakkola, J. Tenenbaum, L. Kaelbling, A. Srivastava,  
207 and P. Agrawal. Compositional foundation models for hierarchical planning. *Advances in*  
208 *Neural Information Processing Systems*, 36, 2024.
- 209 [9] J. Gao, K. Hu, G. Xu, and H. Xu. Can pre-trained text-to-image models generate visual goals  
210 for reinforcement learning? *Advances in Neural Information Processing Systems*, 36, 2024.
- 211 [10] O. Mees, L. Hermann, E. Rosete-Beas, and W. Burgard. Calvin: A benchmark for language-  
212 conditioned policy learning for long-horizon robot manipulation tasks. In *IEEE Robotics and*  
213 *Automation Letters (RAL)*, 2021.
- 214 [11] H. Walke, K. Black, A. Lee, M. J. Kim, M. Du, C. Zheng, T. Zhao, P. Hansen-Estruch,  
215 Q. Vuong, A. He, V. Myers, K. Fang, C. Finn, and S. Levine. Bridgedata v2: A dataset  
216 for robot learning at scale. In *Conference on Robot Learning (CoRL)*, 2023.
- 217 [12] J. Tobin, R. Fong, A. Ray, J. Schneider, W. Zaremba, and P. Abbeel. Domain randomization for  
218 transferring deep neural networks from simulation to the real world. *International Conference*  
219 *on Intelligent Robots and Systems*, 2017.
- 220 [13] C. Zheng, B. Eysenbach, H. Walke, P. Yin, K. Fang, R. Salakhutdinov, and S. Levine. Stabi-  
221 lizing contrastive rl: Techniques for offline goal reaching. *arXiv preprint arXiv:2306.03346*,  
222 2023.
- 223 [14] R. Goyal, S. E. Kahou, V. Michalski, J. Materzynska, S. Westphal, H. Kim, V. Haenel, I. Fru-  
224 end, P. Yianilos, M. Mueller-Freitag, and et al. The “something something” video database for  
225 learning and evaluating visual common sense. In *IEEE international conference on computer*  
226 *vision (ICCV)*, 2017.
- 227 [15] M. Kim, K. Pertsch, S. Karamcheti, T. Xiao, A. Balakrishna, S. Nair, R. Rafailov, E. Foster,  
228 G. Lam, P. Sanketi, Q. Vuong, T. Kollar, B. Burchfiel, R. Tedrake, D. Sadigh, S. Levine,  
229 P. Liang, and C. Finn. Openvla: An open-source vision-language-action model. *arXiv preprint*  
230 *arXiv:2406.09246*, 2024.
- 231 [16] J. Sohl-Dickstein, E. Weiss, N. Maheswaranathan, and S. Ganguli. Deep unsupervised learn-  
232 ing using nonequilibrium thermodynamics. In *International conference on machine learning*,  
233 pages 2256–2265. PMLR, 2015.
- 234 [17] J. Ho, A. Jain, and P. Abbeel. Denoising diffusion probabilistic models. *Advances in neural*  
235 *information processing systems*, 33:6840–6851, 2020.
- 236 [18] A. Vaswani, N. Shazeer, N. Parmar, J. Uszkoreit, L. Jones, A. N. Gomez, Ł. Kaiser, and I. Polo-  
237 sukhin. Attention is all you need. *Advances in neural information processing systems*, 30,  
238 2017.

- 239 [19] A. Brohan, N. Brown, J. Carbajal, Y. Chebotar, J. Dabis, C. Finn, K. Gopalakrishnan, K. Hausman, A. Herzog, J. Hsu, et al. Rt-1: Robotics transformer for real-world control at scale. *arXiv preprint arXiv:2212.06817*, 2022.
- 240  
241
- 242 [20] C. Chi, S. Feng, Y. Du, Z. Xu, E. Cousineau, B. Burchfiel, and S. Song. Diffusion policy: Visuomotor policy learning via action diffusion. *arXiv preprint arXiv:2303.04137*, 2023.
- 243  
244
- 245 [21] A. Brohan, N. Brown, J. Carbajal, Y. Chebotar, X. Chen, K. Choromanski, T. Ding, D. Driess, A. Dubey, C. Finn, et al. Rt-2: Vision-language-action models transfer web knowledge to robotic control. *arXiv preprint arXiv:2307.15818*, 2023.
- 246  
247
- 248 [22] Octo Model Team, D. Ghosh, H. Walke, K. Pertsch, K. Black, O. Mees, S. Dasari, J. Hejna, C. Xu, J. Luo, T. Kreiman, Y. Tan, L. Y. Chen, P. Sanketi, Q. Vuong, T. Xiao, D. Sadigh, C. Finn, and S. Levine. Octo: An open-source generalist robot policy. In *Proceedings of Robotics: Science and Systems*, Delft, Netherlands, 2024.
- 249  
250
- 251 [23] R. Doshi, H. Walke, O. Mees, S. Dasari, and S. Levine. Scaling cross-embodied learning: One policy for manipulation, navigation, locomotion and aviation. In *Conference on Robot Learning*, 2024.
- 252  
253
- 254 [24] M. Zawalski, W. Chen, K. Pertsch, O. Mees, C. Finn, and S. Levine. Robotic control via embodied chain-of-thought reasoning. In *Conference on Robot Learning*, 2024.
- 255  
256
- 257 [25] Z. Mandi, H. Bharadhwaj, V. Moens, S. Song, A. Rajeswaran, and V. Kumar. Cacti: A framework for scalable multi-task multi-scene visual imitation learning. *arXiv preprint arXiv:2212.05711*, 2022.
- 258  
259
- 260 [26] Z. Chen, S. Kiami, A. Gupta, and V. Kumar. Genaug: Retargeting behaviors to unseen situations via generative augmentation. *arXiv preprint arXiv:2302.06671*, 2023.
- 261  
262
- 263 [27] T. Yu, T. Xiao, A. Stone, J. Tompson, A. Brohan, S. Wang, J. Singh, C. Tan, J. Peralta, B. Ichter, et al. Scaling robot learning with semantically imagined experience. *arXiv preprint arXiv:2302.11550*, 2023.
- 264  
265
- 266 [28] A. Stone, T. Xiao, Y. Lu, K. Gopalakrishnan, K.-H. Lee, Q. Vuong, P. Wohlhart, S. Kirmani, B. Zitkovich, F. Xia, et al. Open-world object manipulation using pre-trained vision-language models. *arXiv preprint arXiv:2303.00905*, 2023.
- 267  
268
- 269 [29] A. Peng, I. Sucholutsky, B. Z. Li, T. R. Sumers, T. L. Griffiths, J. Andreas, and J. A. Shah. Learning with language-guided state abstractions. *arXiv preprint arXiv:2402.18759*, 2024.
- 270  
271
- 272 [30] W. Huang, P. Abbeel, D. Pathak, and I. Mordatch. Language models as zero-shot planners: Extracting actionable knowledge for embodied agents. In *International Conference on Machine Learning*, pages 9118–9147. PMLR, 2022.
- 273  
274
- 275 [31] W. Huang, F. Xia, T. Xiao, H. Chan, J. Liang, P. Florence, A. Zeng, J. Tompson, I. Mordatch, Y. Chebotar, et al. Inner monologue: Embodied reasoning through planning with language models. *arXiv preprint arXiv:2207.05608*, 2022.
- 276  
277
- 278 [32] A. Brohan, Y. Chebotar, C. Finn, K. Hausman, A. Herzog, D. Ho, J. Ibarz, A. Irpan, E. Jang, R. Julian, et al. Do as i can, not as i say: Grounding language in robotic affordances. In *Conference on robot learning*, pages 287–318. PMLR, 2023.
- 279  
280
- 281 [33] K. Lin, C. Agia, T. Migimatsu, M. Pavone, and J. Bohg. Text2motion: From natural language instructions to feasible plans. *Autonomous Robots*, 47(8):1345–1365, 2023.
- 282  
283
- 284 [34] Z. Wang, S. Cai, G. Chen, A. Liu, X. Ma, and Y. Liang. Describe, explain, plan and select: Interactive planning with large language models enables open-world multi-task agents. *arXiv preprint arXiv:2302.01560*, 2023.

- 283 [35] S. Fujimoto, D. Meger, and D. Precup. Off-policy deep reinforcement learning without exploration. In *International conference on machine learning*, pages 2052–2062. PMLR, 2019.
- 284
- 285 [36] S. K. S. Ghasemipour, D. Schuurmans, and S. S. Gu. Emaq: Expected-max q-learning operator for simple yet effective offline and online rl. In *International Conference on Machine Learning*, pages 3682–3691. PMLR, 2021.
- 286
- 287
- 288 [37] H. Chen, C. Lu, C. Ying, H. Su, and J. Zhu. Offline reinforcement learning via high-fidelity generative behavior modeling. *arXiv preprint arXiv:2209.14548*, 2022.
- 289
- 290 [38] P. Hansen-Estruch, I. Kostrikov, M. Janner, J. G. Kuba, and S. Levine. Idql: Implicit q-learning as an actor-critic method with diffusion policies. *arXiv preprint arXiv:2304.10573*, 2023.
- 291
- 292 [39] K. Cobbe, V. Kosaraju, M. Bavarian, M. Chen, H. Jun, L. Kaiser, M. Plappert, J. Tworek, J. Hilton, R. Nakano, et al. Training verifiers to solve math word problems. *arXiv preprint arXiv:2110.14168*, 2021.
- 293
- 294
- 295 [40] H. Lightman, V. Kosaraju, Y. Burda, H. Edwards, B. Baker, T. Lee, J. Leike, J. Schulman, I. Sutskever, and K. Cobbe. Let’s verify step by step. *arXiv preprint arXiv:2305.20050*, 2023.
- 296
- 297 [41] A. Hosseini, X. Yuan, N. Malkin, A. Courville, A. Sordoni, and R. Agarwal. V-star: Training verifiers for self-taught reasoners. *arXiv preprint arXiv:2402.06457*, 2024.
- 298
- 299 [42] W. Liu, Y. Du, T. Hermans, S. Chernova, and C. Paxton. Structdiffusion: Language-guided creation of physically-valid structures using unseen objects. *arXiv preprint arXiv:2211.04604*, 2022.
- 300
- 301
- 302 [43] W. Huang, F. Xia, D. Shah, D. Driess, A. Zeng, Y. Lu, P. Florence, I. Mordatch, S. Levine, K. Hausman, et al. Grounded decoding: Guiding text generation with grounded models for robot control. *arXiv preprint arXiv:2303.00855*, 2023.
- 303
- 304
- 305 [44] A. Z. Ren, J. Clark, A. Dixit, M. Itkina, A. Majumdar, and D. Sadigh. Explore until confident: Efficient exploration for embodied question answering. In *Robotics Science and Systems (RSS)*, 2024.
- 306
- 307
- 308 [45] Robots that ask for help: Uncertainty alignment for large language model planners. *arXiv preprint arXiv:2307.01928*, 2023.
- 309
- 310 [46] S. Nair, E. Mitchell, K. Chen, B. Ichter, S. Savarese, and C. Finn. Learning language-conditioned robot behavior from offline data and crowd-sourced annotation. *Conference on Robot Learning (CoRL)*, 2021.
- 311
- 312
- 313 [47] L. P. Kaelbling. Learning to achieve goals. In *IJCAI*, volume 2, pages 1094–8. Citeseer, 1993.
- 314
- 315 [48] T. Schaul, D. Horgan, K. Gregor, and D. Silver. Universal value function approximators. In *International conference on machine learning*, pages 1312–1320. PMLR, 2015.
- 316
- 317 [49] M. Andrychowicz, F. Wolski, A. Ray, J. Schneider, R. Fong, P. Welinder, B. McGrew, J. Tobin, O. Pieter Abbeel, and W. Zaremba. Hindsight experience replay. *Advances in neural information processing systems*, 30, 2017.
- 318
- 319 [50] S. Tellex, N. Gopalan, H. Kress-Gazit, and C. Matuszek. Robots that use language. *Annual Review of Control, Robotics, and Autonomous Systems*, 3:25–55, 2020.
- 320
- 321 [51] S. Stepputtis, J. Campbell, M. Phielipp, S. Lee, C. Baral, and H. Ben Amor. Language-conditioned imitation learning for robot manipulation tasks. *Advances in Neural Information Processing Systems*, 33:13139–13150, 2020.
- 322
- 323
- 324 [52] O. Mees, L. Hermann, and W. Burgard. What matters in language conditioned robotic imitation learning over unstructured data. *IEEE Robotics and Automation Letters (RA-L)*, 7(4):11205–11212, 2022.
- 325
- 326

- 327 [53] O. Mees, J. Borja-Diaz, and W. Burgard. Grounding language with visual affordances over  
328 unstructured data. In *Proceedings of the IEEE International Conference on Robotics and Au-*  
329 *tomation (ICRA)*, London, UK, 2023.
- 330 [54] C. Lynch and P. Sermanet. Language conditioned imitation learning over unstructured data.  
331 *arXiv preprint arXiv:2005.07648*, 2020.
- 332 [55] A. Mandlekar, F. Ramos, B. Boots, S. Savarese, L. Fei-Fei, A. Garg, and D. Fox. Iris: Implicit  
333 reinforcement without interaction at scale for learning control from offline robot manipulation  
334 data. In *2020 IEEE International Conference on Robotics and Automation (ICRA)*, pages  
335 4414–4420. IEEE, 2020.
- 336 [56] S. Park, D. Ghosh, B. Eysenbach, and S. Levine. Hqrl: Offline goal-conditioned rl with latent  
337 states as actions. *Advances in Neural Information Processing Systems*, 36, 2024.
- 338 [57] R. S. Sutton, D. Precup, and S. Singh. Between mdps and semi-mdps: A framework for tem-  
339 poral abstraction in reinforcement learning. *Artificial intelligence*, 112(1-2):181–211, 1999.
- 340 [58] P.-L. Bacon, J. Harb, and D. Precup. The option-critic architecture. In *Proceedings of the AAAI*  
341 *conference on artificial intelligence*, volume 31, 2017.
- 342 [59] J. Schmidhuber. Learning to generate sub-goals for action sequences. In *Artificial neural*  
343 *networks*, pages 967–972, 1991.
- 344 [60] P. Dayan and G. E. Hinton. Feudal reinforcement learning. *Advances in neural information*  
345 *processing systems*, 5, 1992.
- 346 [61] T. D. Kulkarni, K. Narasimhan, A. Saeedi, and J. Tenenbaum. Hierarchical deep reinforce-  
347 *ment learning: Integrating temporal abstraction and intrinsic motivation*. *Advances in neural*  
348 *information processing systems*, 29, 2016.
- 349 [62] A. S. Vezhnevets, S. Osindero, T. Schaul, N. Heess, M. Jaderberg, D. Silver, and  
350 K. Kavukcuoglu. Feudal networks for hierarchical reinforcement learning. In *International*  
351 *conference on machine learning*, pages 3540–3549. PMLR, 2017.
- 352 [63] A. Levy, G. Konidaris, R. Platt, and K. Saenko. Learning multi-level hierarchies with hindsight.  
353 *arXiv preprint arXiv:1712.00948*, 2017.
- 354 [64] O. Nachum, S. S. Gu, H. Lee, and S. Levine. Data-efficient hierarchical reinforcement learning.  
355 *Advances in neural information processing systems*, 31, 2018.
- 356 [65] O. Nachum, S. Gu, H. Lee, and S. Levine. Near-optimal representation learning for hierarchical  
357 reinforcement learning. *arXiv preprint arXiv:1810.01257*, 2018.
- 358 [66] A. Gupta, V. Kumar, C. Lynch, S. Levine, and K. Hausman. Relay policy learning: Solving  
359 long-horizon tasks via imitation and reinforcement learning. *arXiv preprint arXiv:1910.11956*,  
360 2019.
- 361 [67] A. Ajay, A. Kumar, P. Agrawal, S. Levine, and O. Nachum. Opal: Offline primitive discovery  
362 for accelerating offline reinforcement learning. *arXiv preprint arXiv:2010.13611*, 2020.
- 363 [68] C. Lynch, M. Khansari, T. Xiao, V. Kumar, J. Tompson, S. Levine, and P. Sermanet. Learning  
364 latent plans from play. In *Conference on Robot Learning (CoRL)*, pages 1113–1132. PMLR,  
365 2020.
- 366 [69] E. Rosete-Beas, O. Mees, G. Kalweit, J. Boedecker, and W. Burgard. Latent plans for task-  
367 agnostic offline reinforcement learning. In *Conference on Robot Learning*, pages 1838–1849.  
368 PMLR, 2023.

- 369 [70] T. Zhang, S. Guo, T. Tan, X. Hu, and F. Chen. Generating adjacency-constrained subgoals in  
370 hierarchical reinforcement learning. *Advances in neural information processing systems*, 33:  
371 21579–21590, 2020.
- 372 [71] K. Pertsch, Y. Lee, and J. Lim. Accelerating reinforcement learning with learned skill priors.  
373 In *Conference on robot learning*, pages 188–204. PMLR, 2021.
- 374 [72] E. Chane-Sane, C. Schmid, and I. Laptev. Goal-conditioned reinforcement learning with imagined  
375 subgoals. In *International Conference on Machine Learning*, pages 1430–1440. PMLR,  
376 2021.
- 377 [73] N. Savinov, A. Dosovitskiy, and V. Koltun. Semi-parametric topological memory for navigation.  
378 *arXiv preprint arXiv:1803.00653*, 2018.
- 379 [74] B. Eysenbach, R. R. Salakhutdinov, and S. Levine. Search on the replay buffer: Bridging  
380 planning and reinforcement learning. *Advances in neural information processing systems*, 32,  
381 2019.
- 382 [75] S. Nair and C. Finn. Hierarchical foresight: Self-supervised learning of long-horizon tasks via  
383 visual subgoal generation. *arXiv preprint arXiv:1909.05829*, 2019.
- 384 [76] S. Nasiriany, V. Pong, S. Lin, and S. Levine. Planning with goal-conditioned policies. *Ad-*  
385 *vances in Neural Information Processing Systems*, 32, 2019.
- 386 [77] Z. Huang, F. Liu, and H. Su. Mapping state space using landmarks for universal goal reaching.  
387 *Advances in Neural Information Processing Systems*, 32, 2019.
- 388 [78] C. Hoang, S. Sohn, J. Choi, W. Carvalho, and H. Lee. Successor feature landmarks for long-  
389 horizon goal-conditioned reinforcement learning. *Advances in neural information processing*  
390 *systems*, 34:26963–26975, 2021.
- 391 [79] J. Kim, Y. Seo, and J. Shin. Landmark-guided subgoal generation in hierarchical reinforcement  
392 learning. *Advances in neural information processing systems*, 34:28336–28349, 2021.
- 393 [80] L. Zhang, G. Yang, and B. C. Stadie. World model as a graph: Learning latent landmarks  
394 for planning. In *International conference on machine learning*, pages 12611–12620. PMLR,  
395 2021.
- 396 [81] D. Shah, B. Eysenbach, G. Kahn, N. Rhinehart, and S. Levine. Rapid exploration for open-  
397 world navigation with latent goal models. *arXiv preprint arXiv:2104.05859*, 2021.
- 398 [82] K. Fang, P. Yin, A. Nair, and S. Levine. Planning to practice: Efficient online fine-tuning by  
399 composing goals in latent space. In *2022 IEEE/RSJ International Conference on Intelligent*  
400 *Robots and Systems (IROS)*, pages 4076–4083. IEEE, 2022.
- 401 [83] J. Li, C. Tang, M. Tomizuka, and W. Zhan. Hierarchical planning through goal-conditioned  
402 offline reinforcement learning. *IEEE Robotics and Automation Letters*, 7(4):10216–10223,  
403 2022.
- 404 [84] J. Kim, Y. Seo, S. Ahn, K. Son, and J. Shin. Imitating graph-based planning with goal-  
405 conditioned policies. *arXiv preprint arXiv:2303.11166*, 2023.
- 406 [85] K. Fang, P. Yin, A. Nair, H. R. Walke, G. Yan, and S. Levine. Generalization with lossy  
407 affordances: Leveraging broad offline data for learning visuomotor tasks. In *Conference on*  
408 *Robot Learning*, pages 106–117. PMLR, 2023.
- 409 [86] T. Brooks, A. Holynski, and A. A. Efros. Instructpix2pix: Learning to follow image editing  
410 instructions. In *Conference on Computer Vision and Pattern Recognition (CVPR)*, 2023.

- 411 [87] J. Xing, M. Xia, Y. Zhang, H. Chen, W. Yu, H. Liu, X. Wang, T.-T. Wong, and Y. Shan.  
412      Dynamicrafter: Animating open-domain images with video diffusion priors. *arXiv preprint*  
413      *arXiv:2310.12190*, 2023.
- 414 [88] J. Ho and T. Salimans. Classifier-free diffusion guidance. *arXiv preprint arXiv:2207.12598*,  
415      2022.
- 416 [89] Y. Song, J. Sohl-Dickstein, D. P. Kingma, A. Kumar, S. Ermon, and B. Poole. Score-based gen-  
417      erative modeling through stochastic differential equations. *arXiv preprint arXiv:2011.13456*,  
418      2020.
- 419 [90] P. Dhariwal and A. Nichol. Diffusion models beat gans on image synthesis. *Advances in neural*  
420      *information processing systems*, 34:8780–8794, 2021.
- 421 [91] R. Rombach, A. Blattmann, D. Lorenz, P. Esser, and B. Ommer. High-resolution image syn-  
422      thesis with latent diffusion models. In *Proceedings of the IEEE/CVF conference on computer*  
423      *vision and pattern recognition*, pages 10684–10695, 2022.
- 424 [92] E. Perez, F. Strub, H. De Vries, V. Dumoulin, and A. Courville. Film: Visual reasoning with  
425      a general conditioning layer. In *Proceedings of the AAAI conference on artificial intelligence*,  
426      volume 32, 2018.

427 **A Related work**

428 **Generative Models for Robotic Control:** Prior works have explored diverse ways to leverage  
429 generative models, such as diffusion models [16, 17] and Transformers [18], for robotic control.  
430 They have employed highly expressive generative models, potentially pre-trained on Internet-scale  
431 data, for low-level control [19, 20, 21, 22, 23, 24], data augmentation [25, 26, 27], object detec-  
432 tion [28, 29], semantic planning [30, 31, 32, 33, 34], and visual planning [6, 4, 7, 5, 8, 9]. Among  
433 them, our work is most related to prior works that employ image or video prediction models to gen-  
434 erate intermediate subgoal images for the given language task [6, 4, 7, 5, 8, 9]. These works use  
435 diffusion models to convert language instructions into visual subgoal plans, which are then fed into  
436 low-level subgoal-conditioned policies to produce actions. While sensible, this configuration leads  
437 to failures due to the misalignment of the generative models and the low-level policies that control  
438 the robot behavior, as shown in our experiments (section 3).

439 **Rejection Sampling:** One of our key ideas in this paper is based on rejection sampling, where we  
440 sample multiple subgoal proposals from an image or video prediction model and pick the best one  
441 based on a learned subgoal classifier. The idea of test-time rejection sampling has been widely used  
442 in diverse areas of machine learning, such as filtering-based action selection in offline reinforcement  
443 learning (RL) [35, 36, 37, 38], response verification in natural language processing [39, 40, 41], and  
444 planning and exploration in robotics [42, 32, 33, 43, 44]. Previous works in robotics have proposed  
445 several ways to filter out infeasible plans generated by pre-trained foundation models [42, 32, 33, 43,  
446 45]. Unlike these works, we focus on filtering visual subgoals instead of language plans [32, 43, 45],  
447 and do not involve any planning procedures [33] or structural knowledge [42]. While the subgoal  
448 classifier we train resembles the classifier from [46], our classifier differs in two key ways. First, we  
449 use our classifier to filter out “off-task” subgoals, whereas the classifier in [46] is used as a reward  
450 function for training downstream policies. Second, the classifier from [46] is conditioned on the initial  
451 state  $s_0$  and the current state  $s$ , whereas our classifier is conditioned on the current state  $s$  and  
452 a generated subgoal  $g$ .

453 **Goal-Conditioned Policy Learning:** Our method is broadly related to goal-conditioned policy  
454 learning [47, 48, 49], language-conditioned policy learning [50, 51, 52, 53, 54], and hierarchical  
455 control [4, 5, 55, 56, 57, 58]. Most prior works in hierarchical policy learning either train a high-  
456 level policy from scratch that produces subgoals or latent skills [59, 60, 61, 62, 63, 64, 65, 66, 67, 68,  
457 69, 70, 71, 72, 56] or employ subgoal planning [73, 74, 75, 76, 77, 78, 79, 80, 81, 82, 83, 84, 69, 85].  
458 Unlike these works, we do not train a high-level subgoal prediction model from scratch nor involve  
459 a potentially complex planning procedure. Instead, we sample multiple potential subgoals from a  
460 pre-trained (or potentially fine-tuned) image or video prediction model and pick the best one based  
461 on a trained subgoal classifier. Among hierarchical policy methods, perhaps the closest work to  
462 ours is IRIS [55], which trains a conditional variational autoencoder to generate subgoal proposals  
463 and selects the best subgoal that maximizes the task value function. While conceptually similar,  
464 our method differs from IRIS in that we do not assume access to a reward function in order to train  
465 a value function. Our classifier is trained on trajectories consisting only of images and language  
466 descriptions.

467 **Diffusion Model Guidance:** The generative models we consider in our paper [86, 87] are diffusion-  
468 based models trained using classifier-free guidance (CfG) [88]. Although we use a large value for  
469 the language-prompt guidance parameter at inference in our experiments, we find that producing  
470 “off-task” subgoals is still a common failure mode that is not solved by increasing this parameter  
471 alone.

472 Classifier guidance [16, 89, 90] is also a plausible alternative to rejection sampling, but there are  
473 some practical challenges in training a subgoal classifier for this purpose. First, the diffusion models  
474 we consider use latent diffusion [91], and therefore would require training the subgoal classifier to  
475 operate in the latent space of the diffusion model. Second, the subgoal classifier would need to be  
476 trained on noised data in order to guide the diffusion denoising process of the generative model.  
477 Nevertheless, classifier guidance is a potentially appealing direction for future work.

478 **B Preliminaries**

479 We consider the same problem setting as [4], where the goal is for a robot to perform a task de-  
 480 scribed by some previously unseen language command  $l$ . To do this, we consider the same three  
 481 dataset categories as in [4]: (1) language-labeled video clips  $\mathcal{D}_l$  which contain no robot actions; (2)  
 482 language-labeled robot data  $\mathcal{D}_{l,a}$  that includes both language labels and robot actions; (3) unlabeled  
 483 robot data that only includes actions  $\mathcal{D}_a$ . The dataset  $\mathcal{D}_{l,a}$  consists of a set of trajectory and task  
 484 language pairs,  $\{(\tau^n, l^n)\}_{n=1}^N$ , and a trajectory contains a sequence of state,  $s_t^n \in \mathcal{S}$ , and action,  
 485  $a_t^n \in \mathcal{A}$ , pairs,  $\tau^n = (s_0^n, a_0^n, s_1^n, a_1^n, \dots)$ . Given these datasets, we assume access to two learned  
 486 modules:

- 487 1. **a subgoal generation module** from which we can sample multiple possible future sub-  
 488 goals. This can be trained on  $\mathcal{D}_l$  and  $\mathcal{D}_{l,a}$ .
- 489 2. **a low-level goal-reaching policy** that chooses actions to reach generated subgoals. This  
 490 can be trained on  $\mathcal{D}_a$  and/or  $\mathcal{D}_{l,a}$ .

491 Our contribution is a set of approaches to robustify the interface between these two modules.

492 While GHIL-Glue can be applied to any hierarchical imitation learning method consisting of the  
 493 two components mentioned above, in this work we apply GHIL-Glue to two specific algorithms: (1)  
 494 UniPi [5], in which a high-level model generates a subgoal video, and a low-level inverse-dynamics  
 495 model predicts the actions needed to “connect” the images in the video, and (2) SuSIE [4], in which  
 496 a high-level model generates a subgoal image by “editing” the current image observation, and a  
 497 goal-conditioned policy predicts actions to achieve the subgoal image. We define subgoals,  $g \in \mathcal{G}$ ,  
 498 as video or image samples from the high-level models used in these algorithms.

499 **C Additional Discussion of Image Augmentation De-Synchronization**

500 Generated subgoals can contain visual artifacts that degrade the performance of both the low-level  
 501 control policy and the subgoal classifier. This performance degradation results from the distribution  
 502 shift between the subgoal images seen by the policy during training, which come from the robot  
 503 dataset, and the subgoal images seen during inference, which come from the generative model.  
 504 Ideally, the low-level policy and subgoal classifier would be trained on the same distribution of  
 505 *generated* subgoal images that they will see at inference time. However, due to the high degree of  
 506 variance in sampling images from a generative model, there is not a clear way to obtain generated  
 507 subgoal images that match the actual future states reached in trajectories in the training data. To  
 508 address this issue, we identify a simple yet non-obvious data augmentation practice to train the low-  
 509 level policy and subgoal classifier on goals from the robot dataset while also robustifying them to  
 510 visual artifacts in generated subgoals.

511 Applying image augmentation procedures such as random cropping or color jitter during training is a  
 512 standard approach in image-based robot learning methods [12] to improve the robustness of learned  
 513 models to distribution shifts between their training and evaluation domains. More formally, let  $\phi$   
 514 be the set of image augmentation parameters to be randomly sampled from space  $\Phi$ ,  $p_\Phi(\cdot)$  be some  
 515 probability distribution over  $\Phi$ , and let  $\hat{\phi} \sim p_\Phi(\cdot)$  be some realization of augmentations sampled  
 516 from  $p_\Phi(\cdot)$ . Typically, for each training sample, a different value  $\hat{\phi}$  is applied during training to  
 517 make a model robust to any augmentation in the space  $\Phi$ .

518 For both the low-level goal-conditioned policy and the subgoal classifier, each training sample in-  
 519 cludes two images: the current state  $s$  and the corresponding goal  $g$ . Standard practice is to sample  
 520 augmentation parameters  $\hat{\phi}$  and apply them to all images in a given training sample [4, 13], which  
 521 corresponds to applying the same  $\hat{\phi}$  to both  $s$  and  $g$ . In a non-hierarchical policy setting, this makes  
 522 sense, because at inference time  $s$  and  $g$  will both be sampled from the camera observations of the  
 523 current environment instantiation. However, when using an image or video prediction model for  
 524 subgoal generation, at inference time the low-level policy and subgoal classifier will see states from

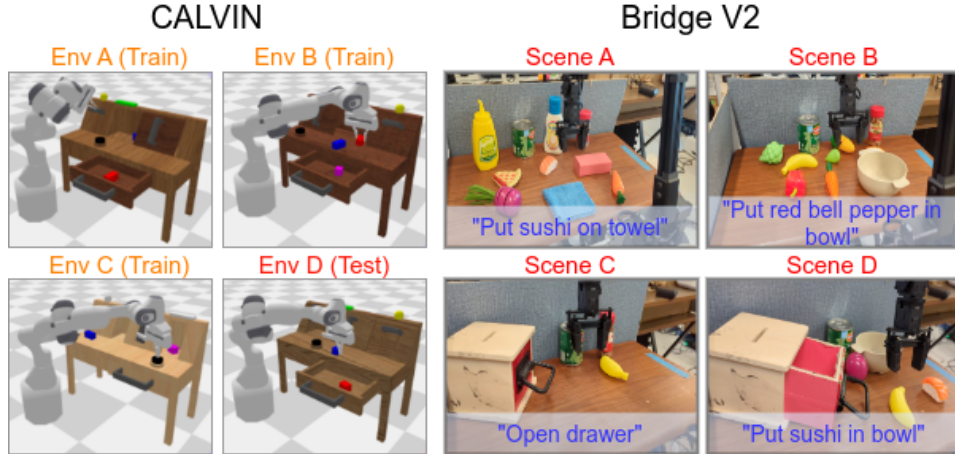
525 the camera observations, but the goals will be generated by the image or video prediction model.  
526 There will often be differences in the visual artifacts between a camera observation  $s$  and the cor-  
527 responding generated subgoal image  $g$ , such as differences in color, contrast, blurriness, and the  
528 shapes of objects, which can degrade the performance of low-level policies and subgoal classifiers.

529 To encourage robustness to this distribution shift, we sample separate augmentation parameters for  
530  $s$  and  $g$ , denoted by  $\hat{\phi}_s$  and  $\hat{\phi}_g$  (i.e., we de-synchronize the image augmentations applied to  $s$  and  
531  $g$ ). Random cropping, brightness shifts, contrast shifts, saturation shifts, and hue shifts comprise  
532 our space of augmentations. Concretely, for each  $s$  and  $g$  pair sampled during training, a different  
533 random crop, brightness, contrast, saturation, and hue shift are applied to  $s$  than are applied to  $g$ .  
534 This forces the low-level policy and the subgoal classifier to learn to make accurate predictions on  
535 ( $s, g$ ) pairs that have differences in visual artifacts.

536 While image augmentations are ubiquitous in robot learning methods, our experiments show that  
537 the standard way of applying image augmentations for goal-conditioned policies and classifiers is  
538 deficient for the hierarchical policy methods that we consider. We also note that augmentation de-  
539 synchronization is applied not only to the policy, but also to the subgoal classifier (section 2.1),  
540 which has a significant impact on overall performance (section 3).

## 541 D Experimental Domains

542 We study the degree to which GHIL-Glue improves existing hierarchical imitation learning algo-  
543 rithms across a number of tasks in simulation and physical experiments that assess zero-shot gen-  
544 eralization. We evaluate our method on the CALVIN [10] simulation benchmark and the Bridge  
545 V2 [11] physical experiment setup with a WidowX250 robot. The experimental domains are visual-  
546 ized in fig. 2.



547 **Figure 2: Experimental Domains.** Simulation Environments (Left): Train/test environments in the CALVIN  
548 simulation benchmark. The environments each have different table textures, furniture positions, and initial con-  
549 figurations of the colored blocks. Each environment contains 34 tasks, each with an associated language instruc-  
550 tion. To test zero-shot generalization, environment D is held out for evaluation. Physical Environments (Right):  
551 We consider four test scenes in the Bridge V2 robot platform with four total language instructions. To test zero-  
shot generalization, these test scenes contain novel objects, language commands, and object configurations not  
seen in the training data.

## 547 E Comparison Algorithms

548 A detailed description of the comparison algorithms referenced in section 3.2 is provided below:

- 549 1. **LCBC Diffusion Policy:** Low-level language-conditioned behavior cloning diffusion pol-  
550 icy [20] trained only on robot trajectories with language annotations. We use the same  
551 implementation as in [4].

- 552     2. **OpenVLA [21]:** A SOTA language-conditioned vision-language-action model (VLA)  
 553     trained on the Open X-Embodiment dataset [2] (which includes the entirety of the Bridge  
 554     V2 dataset).
- 555     3. **SuSIE [4]:** A method which fine-tunes InstructPix2Pix [86], an image-editing diffusion  
 556     model, to generate subgoal images given the current image observation. Low-level control  
 557     is performed using a goal-conditioned policy. For SuSIE and all methods that build on it,  
 558     we predict subgoals 20 steps in the future as in the original paper.
- 559     4. **UniPi [5]:** A method which fine-tunes a language-conditioned video prediction model  
 560     on robot data and then uses an inverse dynamics model for low-level goal reaching. For  
 561     UniPi and all methods that build on it, we predict video sequences of 16 frames. As the  
 562     original UniPi model is not publicly available, we re-implement UniPi by fine-tuning the  
 563     video model from [87].
- 564     5. **GHIL-Glue (SuSIE / UniPi):** GHIL-Glue applied on top of either SuSIE or UniPi. For  
 565     all experiments we implement the subgoal filtering step by sampling four to eight subgoals  
 566     from the high-level video prediction model and selecting amongst them. We directly filter  
 567     the subgoal images generated by the SuSIE model. We filter the video sequences generated  
 568     by the UniPi model based on the final frame of each sequence.
- 569     6. **GHIL-Glue (SuSIE / UniPi) - Subgoal Filtering Only:** GHIL-Glue applied to SuSIE or  
 570     UniPi using subgoal filtering but without augmentation de-synchronization.
- 571     7. **GHIL-Glue (SuSIE / UniPi) - Aug De-sync Only:** GHIL-Glue applied to SuSIE or UniPi  
 572     using augmentation de-synchronization but without subgoal filtering.

## 573 F Discussion of Results

574     **Simulation Experiments:** We present results on the CALVIN benchmark in table 1. Applying  
 575     GHIL-Glue yields significant performance increases for SuSIE and UniPi, increasing the average  
 576     successful task sequence length from **2.94** to **3.69** for SuSIE and from **1.02** to **1.56** for UniPi. **GHIL-**  
 577     **Glue (SuSIE) achieves a new SOTA on CALVIN for policies that use observations from a single**

578     **RGB camera.** The two components of GHIL-Glue (subgoal filtering and image augmentation  
 579     de-synchronization) improve performance when applied individually, but, when applied together, these  
 580     components build on each other, leading to a performance increase greater than the sum of the  
 581     individual benefits. Specifically, for SuSIE, image augmentation de-synchronization and subgoal  
 582     filtering individually yield increases in sequence length of 0.56 and 0.02 respectively, whereas when  
 583     applied together they yield an increase of 0.75. Similarly, for UniPi, the individual improvements  
 584     yield increases in sequence length of 0.08 and 0.34 respectively, compared to an increase of 0.54  
 585     when applied together.

586     When applied alone, image augmentation de-synchronization increases the average successful task  
 587     sequence length from 2.94 to 3.51 for SuSIE and from 1.02 to 1.1 for UniPi. We hypothesize  
 588     that augmentation de-synchronization improves performance a large amount with SuSIE because  
 589     its low-level policy is conditioned on a camera observation image  $s$  from the environment and a  
 590     subgoal image  $g$  generated by the image model. When generalizing to the held-out test environment  
 591     D, the SuSIE image model generates subgoal images with visual discrepancies from the camera  
 592     observation images. In contrast, the UniPi video model predicts a sequence of frames as opposed to a  
 593     single subgoal image. The UniPi low-level policy functions as an inverse dynamics model, choosing  
 594     actions to link between the frames of the generated subgoal video, and is therefore conditioned on  
 595     an  $s$  and  $g$  that both come from the predicted subgoal video.

596     When applied alone, subgoal filtering has a small effect on SuSIE, while on UniPi it increases the  
 597     average successful task sequence length from 1.02 to 1.36. This suggests that unless the SuSIE  
 598     low-level policy is made robust to visual artifacts in generated subgoals, simply selecting the most  
 599     task relevant subgoal is insufficient to improve performance. As discussed previously, the SuSIE

600 low-level policy is more sensitive to visual artifacts in generated subgoals than is the UniPi inverse  
601 dynamics model.

602 **Physical Experiments:** We present results (table 2) comparing GHIL-Glue (SuSIE) to OpenVLA  
603 and SuSIE across four environments on the Bridge V2 robot platform that require interacting with  
604 a number of objects on a cluttered table (fig. 2). These environments require generalizing to novel  
605 scenes, with novel objects, and with novel language commands that are not seen in the Bridge V2  
606 dataset. GHIL-Glue applied to SuSIE outperforms SuSIE across all tasks and outperforms Open-  
607 VLA, a 7-billion parameter SOTA VLA, on 3 out of 4 tasks. Significantly, the baseline SuSIE  
608 implementation does not outperform OpenVLA on a single task, whereas GHIL-Glue (SuSIE) out-  
609 performs OpenVLA on 3 out of 4 tasks, demonstrating that hierarchical goal conditioned architec-  
610 tures with well-tuned interfaces between the high and low-level policies can outperform SOTA VLA  
611 methods on zero-shot generalization tasks.

## 612 G Classifier Training

613 **Training objective:** The classifier is trained using binary cross-entropy loss:

$$\mathcal{J}(\theta) = \mathbb{E}_{(s,g,l) \sim D_l} [\log(f_\theta(s, g, l))] + \mathbb{E}_{(s',g',l') \sim N(D_l)} [1 - \log(f_\theta(s', g', l'))],$$

614 where  $D_l$  is the language-annotated dataset that consists of trajectory and language task pairs, and  
615  $N$  is a function for generating negative examples from the dataset. Given a dataset  $D_l$ ,  $N$  generates  
616 negatives from  $D_l$  in the following ways:

- 617 1. **Wrong Instruction:**  $(s, g, l')$  where  $l'$  is sampled from a different transition than  $s$  and  $g$ .
- 618 2. **Wrong Goal Image:**  $(s, g', l)$  where  $g'$  is sampled from a different transition than  $s$  and  $l$ .
- 619 3. **Reverse Direction:**  $(g, s, l)$ , where the order of the current image observation and the  
620 subgoal image have been switched.

621 Across all our experiments, we sample 50% of each training batch to be positive examples and  
622 50% of each training batch to be negative examples. Of the negative examples, 40% are “wrong  
623 instruction”, 40% are “reverse direction”, and 20% are “wrong goal image”.

624 **Goal sampling:** In a given training tuple  $(s_t, g, l)$ ,  $g$  is sampled by taking the goal image from the  
625  $s_{t+k}$ , where  $k$  is a uniformly sampled integer from 16 to 24.

626 **Network architecture and training hyperparameters:** The classifier network architecture consists  
627 of a ResNet-34 encoder from [11], followed by a two-layer MLP with layers of dimension 256.  
628 Separate encoders are used to encode the image observations and the goal images (parameters are  
629 not shared between the two). Both of these encoders use FiLM conditioning [92] after each residual  
630 block to condition on the language instruction. Classifier networks are trained using a learning rate  
631 of  $3 \times 10^{-4}$  and a batch size of 256 for 100,000 gradient steps. A dropout rate of 0.1 is used.

## 632 H Image Augmentations

633 During training of low-level policy networks and classifier networks, we apply the following aug-  
634 mentations to the image observations and the goal images, in the following order:

- 635 1. Random Resized Crop:
  - 636 • scale: (0.8, 1.0)
  - 637 • ratio: (0.9, 1.1)
- 638 2. Random Brightness Shift:
  - 639 • shift ratio: 0.2

- 640        3. Random Contrast:  
 641            • Contrast range: (0.8, 1.2)  
 642        4. Random Saturation:  
 643            • Saturation range: (0.8, 1.2)  
 644        5. Random Hue:  
 645            • shift ratio: 0.1

646        Figure 3 visualizes examples from the Bridge dataset before and after augmentations are applied:

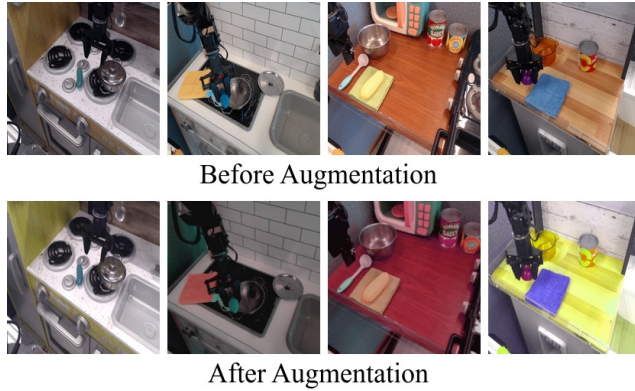


**Figure 3: Image augmentation examples** Examples of images from the Bridge dataset before and after having the image augmentations applied to them that are used during policy and classifier training.

## 647 I Qualitative Analysis

### 648 I.1 Effect of subgoal filtering

649        Although we use classifier-free guidance (CfG) [88] on the image or video generative model with  
 650        respect to the language-prompt at inference in our experiments, we find that producing “off-task”  
 651        subgoals is still a common failure mode that is not solved by increasing the guidance parameter  
 652        alone. In fig. 4, we visualize how subgoal filtering can prevent “off-task” subgoals generated by the  
 653        image or video model from being passed to the low-level control policy.

### 654 I.2 Classifier rankings

655        We show examples of how the classifier network ranks generated goal images on tasks from Scene D  
 656        of our physical experimental domain. Figures 5a, 5b, 5c show examples of the classifier correctly  
 657        ranking the generated goal images (highly ranked images correspond to making progress towards  
 658        correctly completing the language instruction), while fig. 5d shows an example of the classifier  
 659        erroneously giving high rankings to goal images that do not make progress towards completing the  
 660        language instruction. Note that while the classifier scores can be close across various goal images,  
 661        so long as the relative ranking of the generated goal images is correct, then incorrect subgoal images  
 662        will be rejected and correct subgoal images will be passed to the low-level policy.

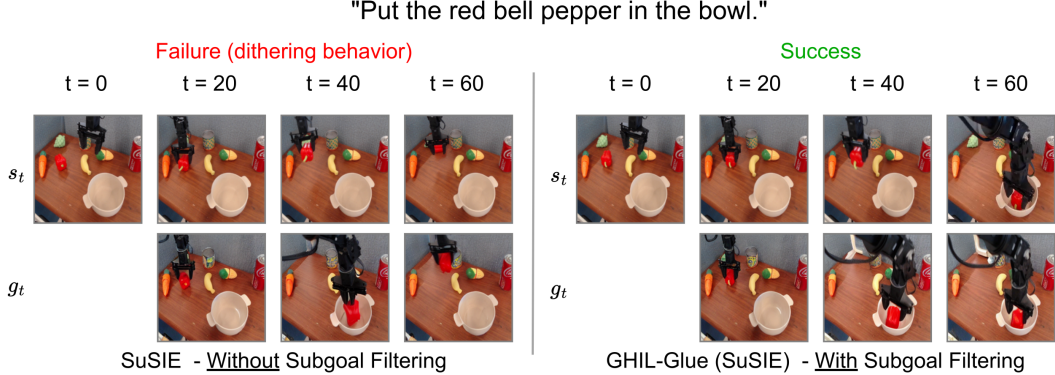


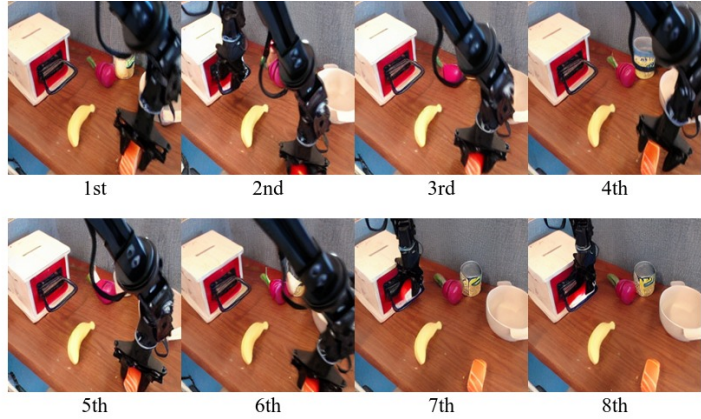
**Figure 4: GHIL-Glue Subgoal Filtering.** We visualize policy rollouts of SuSIE without subgoal filtering vs. GHIL-Glue SuSIE with subgoal filtering. We show the states reached every 20 timesteps (top row) and the corresponding predicted subgoals (bottom row). Without subgoal filtering, the subgoal at  $t = 60$  is not consistent with making progress towards placing the pepper in the bowl, causing the robot to dither and drop the pepper. When subgoal filtering is used, the selected subgoals make iterative progress towards a successful task completion.

**Figure 5: Classifier ranking examples** Examples of the classifier network rankings on 8 generated candidate subgoals given an observation from Scene D of the physical experiments and a language instruction. Note that during GHIL-Glue inference, only the first-ranked subgoal is passed to the low-level policy.

Language instruction:  
*"Put the sushi into the bowl."*



Image Observation



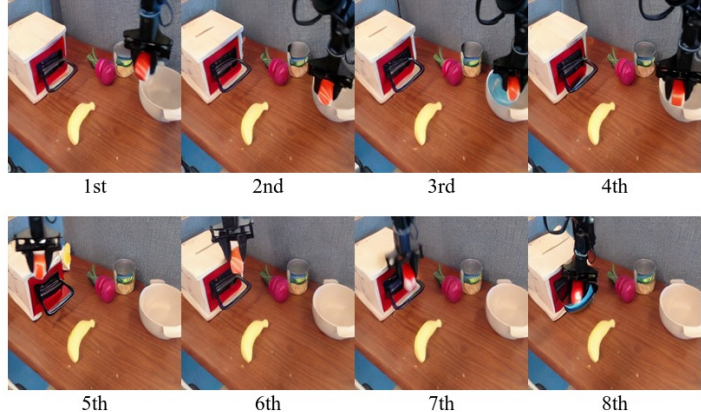
Generated goal images ranked by the classifier

**(a) Correct Example of Classifier Filtering** The classifier correctly ranks the subgoal images where the robot is grasping the sushi higher than the subgoal images where the robot is grasping the drawer handle.

Language instruction:  
*"Put the sushi into the bowl."*



Image Observation



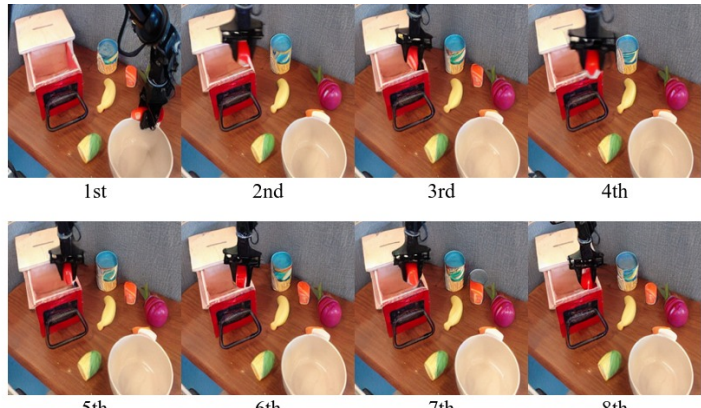
Generated goal images ranked by the classifier

**(b) Correct Example of Classifier Filtering** The classifier correctly ranks the subgoal images where the robot moves to place the grasped sushi into the bowl higher than the subgoal images where the robot moves its gripper towards the drawer handle. It ranks the subgoal image with the hallucinated blue bowl-like artifact last.

Language instruction:  
*"Put the sushi into the bowl."*



Image Observation



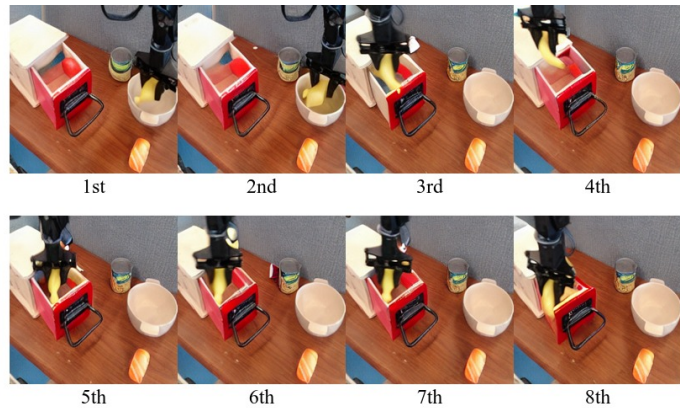
Generated goal images ranked by the classifier

**(c) Correct Example of Classifier Filtering** The classifier correctly ranks the subgoal image highest that shows the robot completing the correct task – only a single generated subgoal image shows the robot placing the sushi into the bowl, while all other generated subgoal images show the robot placing the sushi into the drawer.

Language instruction:  
*"Put the banana into the drawer."*



Image Observation



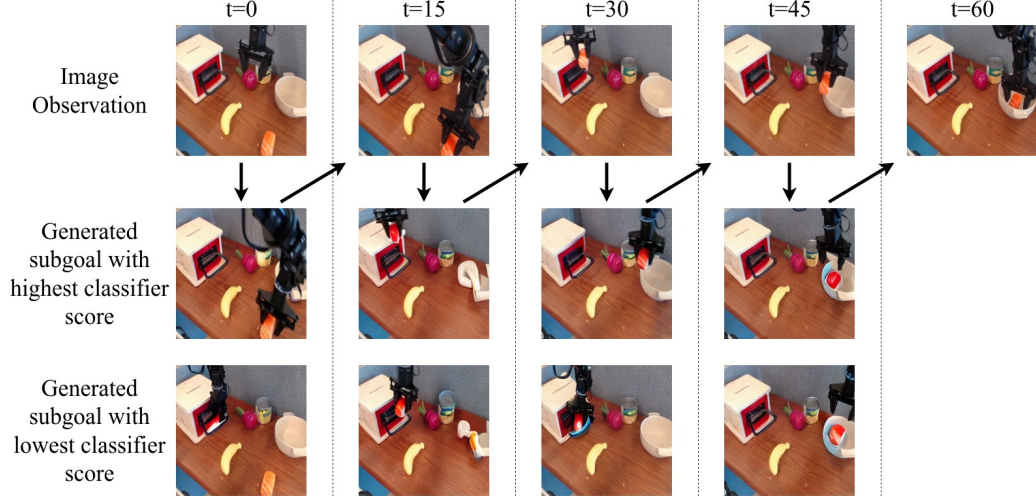
Generated goal images ranked by the classifier

**(d)** The classifier incorrectly ranks the subgoal images higher where the robot is placing the banana into the bowl than it ranks the subgoal images where the robot is placing the banana into the drawer. This could be due to there being a strong bias for placing objects in bowls in the Bridge V2 training data.

663 **I.3 Trajectory Visualizations**

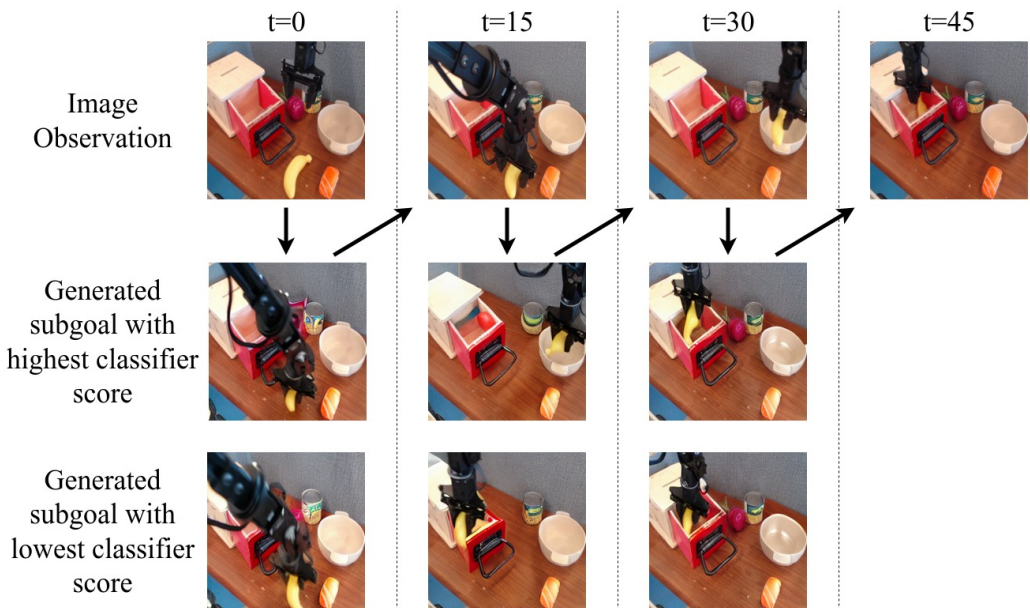
664 We show examples of rollouts of GHIL-Glue (SuSIE) on our physical experiment set up. These  
 665 examples showcase when GHIL-Glue successfully filters out off-task subgoal images (Figure 6a),  
 666 as well as an instance of when GHIL-Glue nearly causes a failure (Figure 6b).

**Figure 6: GHIL-Glue (SuSIE) Trajectory Visualization** Visualization of a rollout of GHIL-Glue (SuSIE) on Scene D in the physical experiments set up. The top row shows the current image observation at every timestep at which the video prediction model is queried. The second and third rows show the highest and lowest ranked generated subgoal images out of the 8 generated subgoal images, as ranked by the classifier. Note that during GHIL-Glue inference, only the first-ranked subgoal is passed to the low-level policy.



Language instruction: "Put the sushi into the bowl."

(a) **"Put the sushi into the bowl."** This rollout shows two examples of the classifier filtering preventing the policy from going off-task: at  $t = 0$ , the lowest ranked generated subgoal shows the gripper grasping the drawer handle instead of moving to grasp the sushi; at  $t = 30$ , the lowest ranked generated subgoal shows the gripper moving towards the drawer handle instead of towards placing the sushi into the bowl. Note the hallucinated objects and artifacts visible in the goal images at  $t = 15, 30, 45$ . Augmentation de-synchronization helps to make the low-level policy and classifier robust to hallucinated artifacts such as these.



Language instruction: "*Put the banana into the drawer.*"

**(b) “Put the banana into the drawer.”** In this rollout, classifier filtering fails and causes a near-miss. At  $t = 15$ , the classifier ranks a subgoal image highest that shows the robot placing the banana into the bowl instead of the drawer. However, at  $t = 30$ , when the robot reaches the state specified by this subgoal image, the subsequent generated subgoals all show the robot correctly placing the banana into the drawer. Although, as in this example, the classifier network can occasionally rank incorrect subgoal images higher than correct subgoal images, such errors occur infrequently as GHIL-Glue (SuSIE/UniPi) outperforms base-SuSIE/UniPi across all of our physical and simulated experiments.

667 **I.4 Qualitative Analysis of Augmentation De-synchronization**

668 We see that when applying aug-  
 669 mentation de-synchronization, the  
 670 number of failures due to low-  
 671 level policy errors (missed grasps,  
 672 dropping held objects, etc.) de-  
 673 creases, indicating that augmentation  
 674 de-synchronization is important for  
 675 the low-level policy to be able to cor-  
 676 rectly interpret and follow the sub-  
 677 goal images generated by the video  
 678 prediction model. This is particularly  
 679 important in domains where there is  
 680 a large visual generalization gap be-  
 681 tween the training data and the eval-  
 682 uation tasks. For example, in the  
 683 CALVIN benchmark, the colors and  
 684 shapes of objects differ between the  
 685 training and evaluation scenes. This  
 686 difference causes the subgoals gener-  
 687 ated by the video prediction model to  
 688 often contain objects with incorrect shapes and colors (Figure 7). Augmentation de-synchronization  
 689 seems to be critical to allowing the low-level policy to be robust to these hallucinations and artifacts.

Language Instruction: "Go push the red block left."

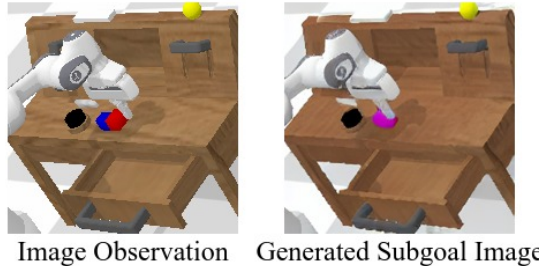


**Figure 7: Generated Subgoal Image on CALVIN** A subgoal image generated by the SuSIE video model on the unseen environment D of the CALVIN benchmark. The colors and shapes of objects are different in each of the four CALVIN environments, and since the model was not trained on data from environment D, it often generates images with incorrect shapes and colors. Augmentation de-synchronization is important for the low-level policy and classifier to be able to handle these mismatches between image observations and corresponding generated subgoal images.

690 **J Number of Candidate Subgoals**

691 We conduct an ablation over the number of candidate subgoals used for subgoal filtering in GHIL-  
 692 Glue (SuSIE) in the CALVIN benchmark. We find that GHIL-Glue (SuSIE) achieves similar per-  
 693 formance whether 4, 8, or 16 candidate subgoals are used. In our main results (section 3.3), we  
 694 report the performance of GHIL-Glue (SuSIE) on the CALVIN benchmark when using 8 candidate  
 695 subgoals for filtering. For GHIL-Glue (UniPi) on the CALVIN benchmark, we use 4 candidate sub-  
 696 goals for filtering, due to the increased computation burden of generating video subgoals with the  
 697 UniPi video model vs. generating image subgoals with the SuSIE image model. In our physical  
 698 experiments, we run GHIL-Glue (SuSIE) using 4 candidate subgoals for filtering.

| Method                         | Tasks completed in a row |              |              |              |              |             |
|--------------------------------|--------------------------|--------------|--------------|--------------|--------------|-------------|
|                                | 1                        | 2            | 3            | 4            | 5            | Avg. Len.   |
| GHIL-Glue (SuSIE) - 4 samples  | 95.2%                    | 86.0%        | 71.2%        | 60.5%        | 50.0%        | 3.63        |
| GHIL-Glue (SuSIE) - 8 samples  | <b>95.2%</b>             | <b>88.5%</b> | <b>73.2%</b> | <b>62.5%</b> | <b>49.8%</b> | <b>3.69</b> |
| GHIL-Glue (SuSIE) - 16 samples | 95.0%                    | 86.5%        | 72.8%        | 60.8%        | 48.0%        | 3.63        |

**Table 3: Effect of Number of Candidate Goal Images Sampled in GHIL-Glue (SuSIE)** Success rates on the validation tasks from environment D of the CALVIN Challenge when using GHIL-Glue (SuSIE) when using 4, 8, or 16 candidate goal images with classifier filtering. Results are averaged across 4 random seeds. Results are similar across all numbers of samples, with 8 samples performing the best by a slight margin.